Available online at www.sciencedirect.com

ScienceDirect

MATTER AND RADIATION AT EXTREMES

Matter and Radiation at Extremes 1 (2016) 135–152

www.journals.elsevier.com/matter-and-radiation-at-extremes

Review article

Theoretical and numerical research of wire array Z-pinch and dynamic hohlraum at IAPCM

Ning Ding*, Yang Zhang, Delong Xiao, Jiming Wu, Zihuan Dai, Li Yin, Zhiming Gao, Shunkai Sun, Chuang Xue, Cheng Ning, Xiaojian Shu, Jianguo Wang

Institute of Applied Physics and Computational Mathematics, P.O. Box 8009, Beijing 100088, PR China

Received 4 April 2016; revised 5 May 2016; accepted 10 May 2016
Available online 14 June 2016

Abstract

Dense Z-pinch plasmas are powerful and energy-efficient laboratory sources of X-rays, and show the possibility to drive inertial confinement fusion (ICF). Recent advances in wire-array Z-pinch and Z-pinch dynamic hohlraum (ZPDH) researches at the Institute of Applied Physics and Computational Mathematics are presented in this paper. Models are setup to study different physical processes. A full circuit model (FCM) was used to study the coupling between Z-pinch implosion and generator discharge. A mass injection model with azimuthal modulation was setup to simulate the wire-array plasma initiation, and the two-dimensional MHD code MARED was developed to investigate the Z-pinch implosion, MRT instability, stagnation and radiation. Implosions of nested and quasi-spherical wire arrays were also investigated theoretically and numerically. Key processes of ZPDH, such as the array–foam interaction, formation of the hohlraum radiation, as well as the following capsule ablation and implosion, were analyzed with different radiation magneto-hydrodynamics (RMHD) codes. An integrated 2D RMHD simulation of dynamic hohlraum driven capsule implosion provides us the physical insights of wire-array plasma acceleration, shock generation and propagation, hohlraum formation, radiation ablation, and fuel compression.

PACS Codes: 52.59.Qy; 52.58.Lq; 52.65.-y; 52.65.Kj

Keywords: Wire-array; Z-pinch; Dynamic holhraum; Inertial confinement fusion (ICF)

1. Introduction

Fast Z-pinch has produced the most powerful X-ray pulse in laboratory plasmas by imploding a cylindrical wire-array with a 100 ns MA-level pulse current [1]. In the late 1990s, on the world's most powerful electrical pulse power generator, the 20 MA Z machine at Sandia National Laboratories, 200 TW 2 MJ bursts of soft-X-ray radiation have been produced via single wire array implosion [2]. A higher record of (280 ± 40) TW was achieved later by using a nested-wire array, whose energy transition efficiency exceeded 15% [3], which showed the great potential of using Z-pinch implosions to drive inertial confinement fusion (ICF). The Z-pinch dynamic hohlraum (ZPDH) is one of the potential schemes to indirect-drive ICF, which employs a high-atomic-number annular Z-pinch plasma imploding onto a cylindrical low-density foam [4–7]. The impact launches a radiating shock, which is the main radiation source heating the hohlraum and driving the ICF capsule to ignition [8]. The ZPDH concept is confirmed by experiments on the 20 MA Z machine, in which the brightness temperature of hohlraum radiation was about 215 eV [8], and 3.5×10^{11} DD thermonuclear neutron yield has been obtained with a Be + CH capsule filled with deuterium gas [9]. In 2010, a so-called magnetized liner inertial fusion (MagLIF) concept was proposed [10], in which a

* Corresponding author.
E-mail address: ding_ning@iapcm.ac.cn (N. Ding).
Peer review under responsibility of Science and Technology Information Center, China Academy of Engineering Physics.

http://dx.doi.org/10.1016/j.mre.2016.06.001

beryllium liner is imploded to directly compress the DT fuel, and the fuel is magnetized by an external current coil and preheated by a laser pulse to lower the required convergence. Until 2014, more than 8 integrated MagLIF experiments have been carried out on the ZR machine, and more than 10^{12} DD Neutron yield was gained.

A typical Z pinch can be qualitatively divided into four stages: the pulsed power formation, wire initiation, implosion, and stagnation. In the first stage, the electrical energy stored into the generator capacitor is released as a power pulse. It is compressed further by the transmission line, which results in a very short but powerful current imposed on the load region. In the second stage, the metal wires get vaporized and ionized due to the Joule heating, and become plasma during the ablation. Small part of them is blown towards the axis and forms the precursor plasma. The rest of plasma, as well as some residual wire cores, is still at the initial position until the $\boldsymbol{J} \times \boldsymbol{B}$ force is large enough to accelerate them, which is regarded as the start of the implosion stage. During the implosion, the plasma can be sped up to 10^7 cm/s, and the magnetic energy is converted into plasma kinetic energy. While the high speed plasma stagnates on the axis, it is compressed into a very dense state, causing the production of powerful x-ray radiation. When a Z-pinch implosion is used to drive ICF indirectly, the kinetic or radiation energy is used to form a holhraum. The high temperature holhraum will create a symmetrical radiation environment, which irradiates the ICF capsule to implode uniformly and get ignited at last.

In recent years, many Chinese institutes and universities devoted themselves into the research of wire-array Z-pinches. Several low current generators, such as the Qiangguang-I facility in the Northwest Institute of Nuclear Technology [11,12], the Yang facility in the Institute of Fluid Physics [13], and the PPG-I facility in the Tsinghua University [14], have been setup and used for Z-pinch studies. Currently, the ~8 MA PTS (Primary Test Stand) facility in China has been completed, which provides a powerful experimental platform of relatively large drive current for researches of ZPDH [15−17]. In 2000, the remarkable development of Z pinch physics attracted our attention, and a research team focusing on the theoretical and numerical study of Z pinch and Z-pinch drive ICF was founded in the Institute of Applied Physics and Computational Mathematics (IAPCM).

1D- and 2D- MHD codes were developed by us to study the key processes of Z pinch dynamics and radiation. Since the Z-pinch implosion is strongly coupled with the generator, a full circuit model (FCM) and several simplified models were setup to study the discharge and pulse compression of the generator and its energy coupling with the load and the implosion process. To get a reasonable load initial condition for the 1D and 2D MHD simulation in the (r, z) plane, we studied the wire-array ablation process with a 2D (r, θ) mass injection model, which enables us to predict whether or not a continuous plasma shell is formed before the main implosion happens. We paid a lot of attention on the magneto-Rayleigh-Taylor (MRT) instability. Several potential stabilization methods were studied theoretically and numerically, one of which is the nested wire-array. According to Ding et al.'s work [18], the implosion of nested wire-array have different modes depending on the initial load configuration and inductance. Detailed 2D numerical study were carried out by Huang et al. in the (r, θ) plane [19]. As a valuable laboratory X-ray resource, the most important stages of Z-pinch are the stagnation and radiation. The 2D radiation magneto-hydrodynamics (RMHD) code MARED on the structured quadrilateral mesh was the first one used to study these processes, and a 1D RMHD code CRMHA with more detailed radiation model was setup later to reinforce the research. In order to deal with more complex geometry configuration for Z-pinch models, we also develop a new 2D RMHD code MARED-U which is based on the arbitrary polygonal meshes. Besides the classical column Z pinch, we also studied the dynamics of quasi-spherical Z-pinch implosion and the method of getting it with wire array load and 100 ns fast Z-pinch generator. Since 2010, we paid more attention on the ZPDH physics. The array−foam interaction, formation of the hohlraum radiation, as well as the following capsule ablation and implosion, were analyzed with different RMHD codes. At the same time, to get a comprehensive understanding and a complete physics image of the ZPDH implosion, an integrated 2D simulation capability was setup, which enables us to simulate the whole process of ZPDH from the generator discharge to the ICF capsule implosion. Besides these works, numerical algorithms for radiation diffusion equation were investigated in recent years, and most of them were successfully employed into RMHD codes such as the MARED and MARED-U (See references [20−26] for details).

In this paper, we describe recent advances in theoretical and numerical wire array Z-pinch and ZPDH researches at the Institute of Applied Physics and Computational Mathematics. In the second section, the modeling of the pulsed power system and its coupled results with Z-pinch simulations are presented. In the following three sections, simulation studies on the ablation and initialization of wire arrays, the MRT instability, and stagnation and X-ray radiation are introduced respectively. In the sixth and seventh sections, the implosion of nested wire-arrays, as well as the quasi-spherical wire-arrays, are presented as a complementary study to the typical single array implosion. In the eighth section, we show our recent theoretical and numerical results on the dynamic hohlraum (DH) and DH-driven ICF. At last, a summary of our previous work and a plan for the future study are laid out.

2. Pulsed power system and circuit modeling

In the last 30 years, the pulsed-power technique has experienced great development, which enables new generation drivers to provide enormous power to the Z pinch implosion. Famous generators devoted to the Z-pinch and Z-pinch drive ICF researches include the 10 MA Saturn generator [27,28] and the 20/26 MA Z/ZR machine [3] in the Sandia National Laboratories, and the 5 MA Angara-5-1 facility in the Troistsk Institute for Innovation and Fusion research [29]. Great works were also done on small devices with peak current about 1 MA or less, such as the MAGPIE [30] in the Imperial College, the

Qiangguang-I facility in the Northwest Institute of Nuclear Technology [11,12], and the PPG-I in the Tsinghua university [14]. The new generation driver of China, 10 MA PTS facility [15–17], was founded in 2013, based on which a series of theoretical and experimental works were carried out for the Z-pinch and ZPDH studies.

A pulsed power machine can release the stored electrical energy as a power pulse, which will be compressed gradually when it passes the switch-controlled transmission line. As the pulse width is shortened, the power increases, and finally a 100 ns wide, tens of MA current is formed in the load region. Since the Z-pinch implosion is strongly coupled to the generator, circuit models [11,16,17,31] were setup and coupled with RMHD models to realize the integrated simulation from generator discharge to the Z-pinch implosion and radiation. Thus, circuit simulation is not only an important tool for the driver design, operation and maintenance, but also an effective means for experimental design and analysis. Early circuit model at Sandia for simulating the Z device is SCREAMER [3], during the refurbishment of Z, Bertha code was developed to adapt the variations of the output water transmission line structures. Besides these codes, PSPICE software is also used to study generator discharge behavior.

Recently, we developed a full circuit model (FCM) [11,17] to model the typical single-module or multiple-module drivers for Z-pinch studies, which can be coupled with the RMHD model for the load simulation studies. According to the characteristics of electromagnetic pulse inside the driver, we use voltage and current, instead of the electric field and magnetic field, to describe the discharge process. Systems such as the primary energy storage, switches and load, are treated as lumped parameter circuit elements, while the transmission line is regarded as a distributed parameter circuit element. By connecting these circuit elements in series or parallel combination, we can get the FCMs for different drivers.

Fig. 1 shows the sketch of the FCM simulation of the 10 MA PTS facility, whose structure is shown as well. The PTS facility contains 24 modules in parallel, each one of which is composed of Marx generator, intermediate storage (IS) capacitor, laser-triggered gas switch (LTGS), pulse forming line (PFL), water self-breakdown switch (WS) and the tri-plate output transmission lines (T_{in} and T_{out}). Once discharged, the electric energy is released from the Marx bank, and compressed/amplified in the transmission lines, and then the high-power electromagnetic pulse is formed in the PFLs and T_{in}s. The pulses converged at the insulator stack and vacuum zone, drive the central short-circuit load to achieve high current Z-pinch implosion. Fig. 2 illustrates the measured and simulated 24-modules averaged voltage at different position, and the electromagnetic power is shown as well. The capacitors of the Marx bank are charged at 65 kV, and the 2 cm diameter wire array has a liner mass density of 1.246 mg/cm. It is seen that as the rise time of the pulse is compressed from 620 ns to 70 ns (from IS to Stack), the peak power increases from 4.2 TW to 12.9 TW.

Fig. 2 also compares the simulation results with the experimental results: the 24-modules averaged voltage waveform (a) and the current waveform (b). Using the measured voltage and current near the insulation stack, we reconstruct the incident and reflected voltage waveform, and get a simplified circuit model of the PTS facility (see Fig. 3 (a)). V_0 is the equivalent voltage reconstructed with experimental data of shot # 0081, # 0125, and # 0128, whose peak voltage is 3.3 MV and the rise time (from 10% to 100%) is about 60 ns. $R_0 = 0.156\ \Omega$ is the equivalent impedance derived from the paralleled impedance of tri-plate. According to the position of the actual leakage current, the equivalent inductance of the outer magnetically insulated transmission line is set as $L_m = 12–15$ nH. The typical value of inner magnetically insulated transmission line inductance L_0 is about 2–5 nH, which should be modified with the load electrode parameters. During the implosion, the load inductance and resistance will change with the plasma status, which can be obtained from Z-pinch MHD codes coupled with the FCM. Fig. 3(b) shows the simulated the kinetic energy and the load current of shot # 0081, # 0125, # 0128 with a thin shell Z-pinch model [28], which shows satisfying agreement with the measured current.

3. Ablation and initialization

As the current flows through the metal wire, the material on the wire surface experiences complicated phase transition processes and forms ablated plasmas. These plasmas are accelerated toward the array axis by magnetic pressure and accumulate there to form a precursor column, while the cold-dense wire cores are stable in their original positions and keep ablating. Experimental results show that the basic processes of wire-array ablation on the 20-MA Z machine [32] are similar to those on the smaller current facilities such as ANGARA

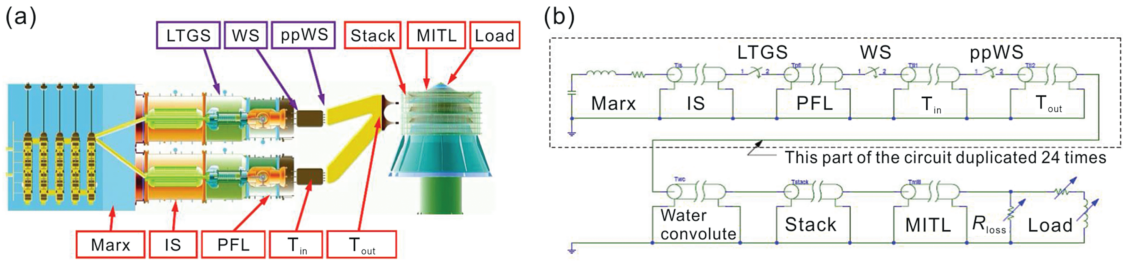

Fig. 1. Schematic structure and circuit model of PTS.

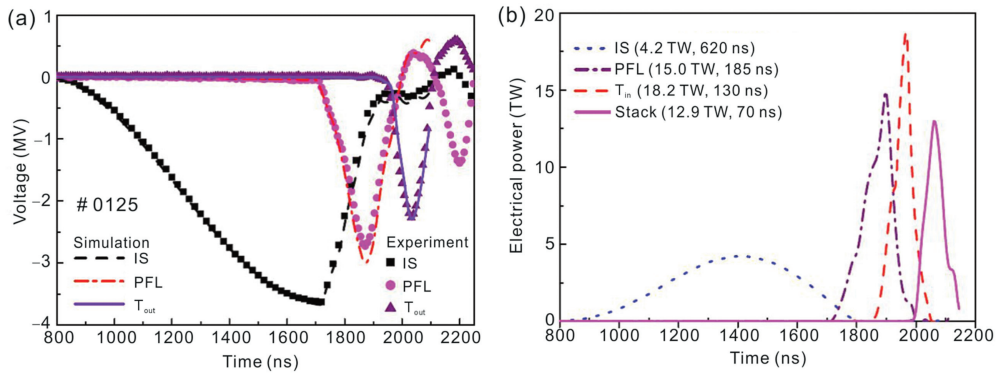

Fig. 2. Comparing the simulation results with the experimental results: the 24-modules averaged voltage waveform (a) and the current waveform (b).

[33], MAGPIE [34] and COBRA [35]. The ablation rate of wire core is axially nonuniform, and the ablated plasmas will carry a significant fraction of current. Actually, the ablation dynamics determine the initial distribution of mass and current density of the implosion, so it plays an important role in the eventual X-ray production of the pinch.

Although many important details of the ablation process are not understood yet because of the difficulties in experimental measurement and simulation, some phenomenological ablation models [34,36] are established, which can give reasonable ablation rate compared to the experiments results. Lebedev et al. have setup a rocket model [34] by assuming the wires represent a series of stationary plasma source at the initial radius and the ablated plasmas fly inward with a constant velocity. A more complex model called as mass injection magneto-hydrodynamic(MHD) model [36–38] were established, in which the movement of ablated plasma is calculated within an ideal MHD frame. By multiplying an axial perturbation coefficient to the 1D ablation rate, the ablation process in 2D (r, z) plane was studied numerically in [39] and achieved similar current waveform and implosion time to the experimental data.

Recently, precursor studies [40,41] show that the current flow through the precursor is strongly influenced by the wire number. To analyze the formation of the precursor current and its relationship with the initial conditions, we extended the 1D mass injection MHD model into 2D (r, θ) plane and used it to simulate the ablation process of the Al wire arrays on 1 MA facility [42,43]. We focused on the 2D image of the ablated-plasma dynamics and the distribution of magnetic fields, trying to understand the distribution of current density in (r, θ) plane from the point of view of the convection of magnetic field, and investigate the relationship between the variables above and the initial conditions of the wire array.

Fig. 4 illustrates the mass injection model in our simulations. The mass ablation rate, i.e., the mass injected per unit area and per unit time at the boundary, is defined as

$$\begin{aligned} \dot{m}(\theta,t) &= \dot{m}_0(t)\varepsilon(\theta), \\ \dot{m}_0(t) &= k\left(\frac{I[\mathrm{MA}]}{R_0[\mathrm{cm}]}\right)^{\mu}\left(\frac{d}{D_g}\right)^{1-\mu/3}, \\ \varepsilon(\theta) &= \sum_{n=1}^{N}\frac{2\pi R_0}{N}\{1+\cos[R_0(\theta-\theta_n)/r_c]\}, \end{aligned} \tag{1}$$

where $\dot{m}_0$ is the 1D mass ablation rate, N and θ_n are the number of wires and the azimuthal coordinate of the n^{th} wire, respectively. r_c is the radius of the wire core which only depends on the wire material. $\varepsilon(\theta)$ is an artificial modulation coefficient that modulates the ablation rate azimuthally.

The ablation dynamics of 16-Al-wire array with an initial radius of 0.8 cm is presented in Fig. 5. Firstly, plasma streams injected from the boundary flow toward the array axis, the regions of high density are close to the position of wire. Secondly, the coronal plasmas arrive at the axis and form a precusor with a radius of 0.2–0.3 cm. Then, the precursor is compressed and a narrow column with higher density is observed at the axis. Finally, the column reaches a minimum radius about 0.07 cm and then begins to expand slowly.

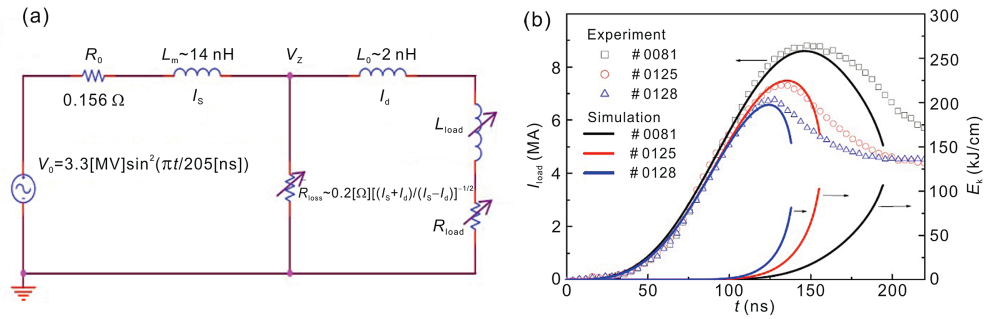

Fig. 3. (a) PTS simplified circuit model; (b) The simulated load current and line kinetic energy by a thin shell code coupled with the FCM.

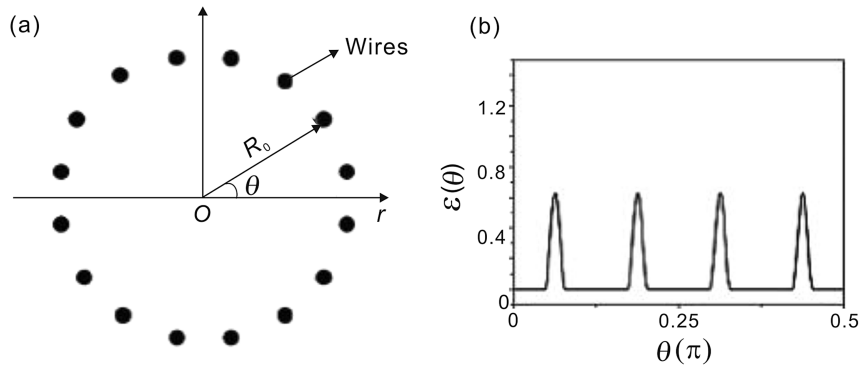

Fig. 4. (a) The cross section of wire array for 16 Al wires and (b) the corresponding azimuthal modulation coefficient $\varepsilon(\theta)(0 \le \theta \le \pi/2)$.

Fig. 6 shows distributions of plasma density, velocity, magnetic field and current density when the ablation streams are just arriving at the axis. Since the radial flow velocity at the edge of the streams is higher than that at the center, the magnetic fields between wires propagate into the interior of wire arrays faster than those inside the streams. Therefore, the field lines have a distinct curvature near the center of ablation center, and the axial current density calculated is mainly confined to the high density region of the streams.

From our simulation results, the dependence of the maximum radial velocity V_a on the ratio of interwire gap/core size D_g/d can be approximately expressed by the formula $V_a = 1.61 \times 10^7\left[(1 - 0.8e^{(-D_g/3.8d)})\right]$, which is similar to that obtained from the experimental observations on MAGPIE [44]. Previous studies have shown that the existence of the precursor column resulted in higher X-ray power [45]. If the interwire separation is too small, the radial velocity of ablated plasmas would be very low and the precursor column would not be formed before the implosion phase and that might lead to decrease in X-ray power. The calculational results can explain the experimental observation that the X-ray power decreases once a critical wire number is exceeded.

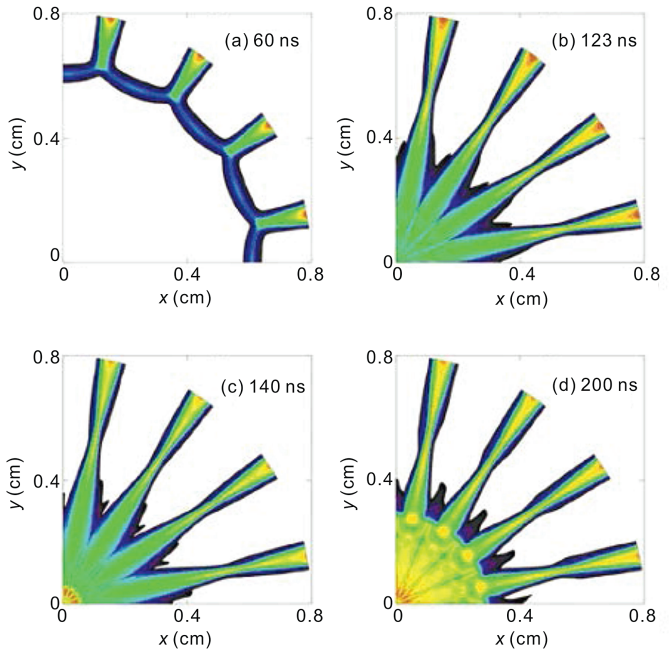

Fig. 5. Distribution of plasma mass density at different times.

The current carried by the precursor plasmas can affect the implosion process of wire array Z-pinch and can be diagnosed in experiment by magnetic probe. For the first time, we analyzed the origin of the precursor current from the point of view of the convection of B-field in (r, θ) plane and assessed precursor current as a function of the wire array parameters. Furthermore, the simulation results can be compared to the experimental results. Simulation results show that for a certain drive current and array radius, the fraction of the precursor current decreases with the increase of wires number (see Fig. Fig. 7). On the other hand, when the inter-wire gap is fixed, the precursor current declines in the Z-pinch of wire array with larger initial radius.

4. The MRT instability

Dense Z-pinch plasmas are powerful and energy-efficient laboratory sources of X-rays, and are extensively used in inertial confinement fusion research, laboratory astrophysics, and high energy density physics. However, the X-ray power generated from Z-pinch implosion is limited by the magneto-Rayleigh-Taylor (MRT) instabilities, caused by the magnetic acceleration of the load plasma during the implosion. According to Haines's model [46], the growth of MRT instability undergoes two stages. In the linear stage, the initial seed grows exponentially with a growth rate proportional to $(g/\lambda)^{1/2}$, where g is the axially inward acceleration of the plasma and λ is the perturbation wavelength. When the amplitude becomes comparable to the wavelength, nonlinear effects become important and the classic bubble and spike structure evolves, broadening the plasma shell [28,47,48]. Hussey et al. [49] have shown that for finite thickness shells, the dominant wavelengths are on the order of the shell thickness, typically a few mm. For severe MRT growth, the bubbles can eventually break through the shell, leading to mass and current leakage ahead of the bulk of the imploding plasma and subsequent loss of driving force. This coupled with shell broadening, limits the compression simultaneity and uniformity of the pinch.

The growth of the MRT instability in the Z-pinch implosions was widely discussed theoretically and numerically. Latham et al. [50] attributed the surface instabilities found in

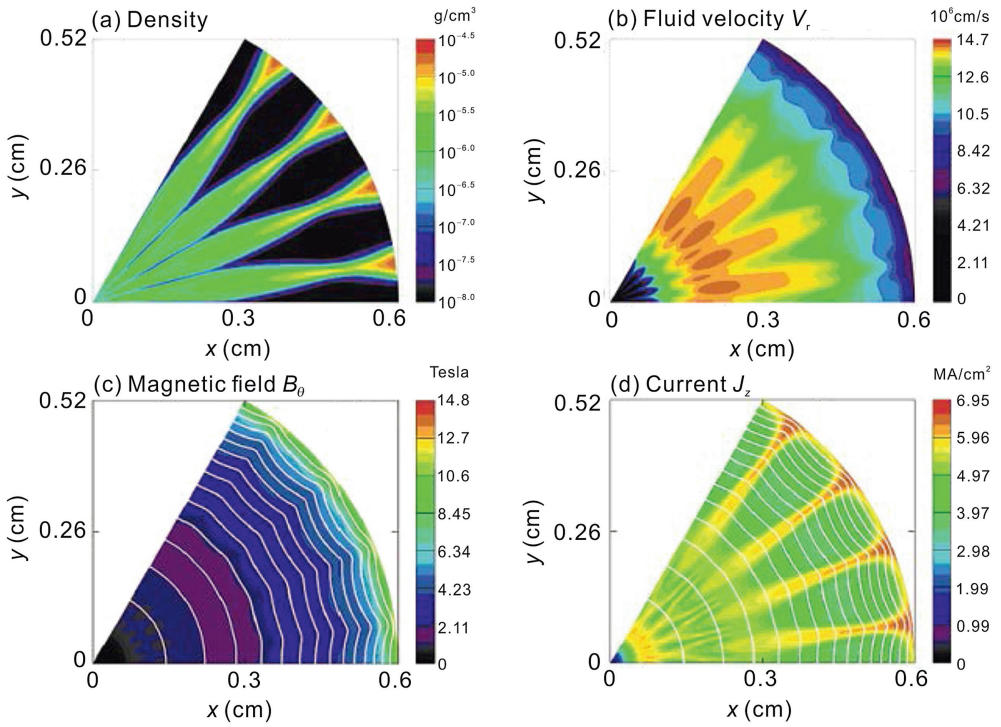

Fig. 6. Distributions of (a) plasma density, (b) radial velocity, (c) magnetic field and (d) current density overlapped by magnetic field when the ablation streams are just arriving at the axis.

a dynamic Z-pinch to MRT for the first time, and growth rates were measured for the wavelengths found. Experimental results at the Sandia National Laboratory (e.g., Sanford et al. [27]) have shown that the X-ray power of Z-pinches increases as the number of wires n employed is increased, with a sharper increase in power when the wire gap is below a critical value. According to these phenomena, Haines setup a heuristic model of wire array that can not only predict the perturbation development in a simple and reasonable way, but also show how the initial perturbations that lead to the Rayleigh-Taylor instability scale as $n^{-1/2}$, where n is the wire number [46]. Potential mitigation effects from the sheared flow, finite ion Larmor radius, viscosity, axial magnetic field, and profiled density, were discussed analytically during the last 20 years. At the same time, MRT instability's effects on the Z-pinch stagnation and radiation were studied numerically, which has been found to provide good matches with experiments. Peterson [47,51–53] has successfully shown agreement in radiation quantities and physical appearance using a random density seed for loads on four different experimental machines, Pegasus [47], Procyon [51], Saturn [52], and Z [53]. Hammer [54], and Douglas [55] have also successfully modeled Saturn experiments using a random density seed. These calculations showed that the MRT instability alone describes the majority of the pinch dynamics and that only a single variable (the initial perturbation amplitude) is necessary to accurately model the experimental data without resorting to modified or anomalous physical parameters.

In China, professor Qiu, Huang, and Jian [56–58] from the Southwestern Institute of Physics studied theoretically the stabilization of sheared axial flow, finite Larmor radius, and

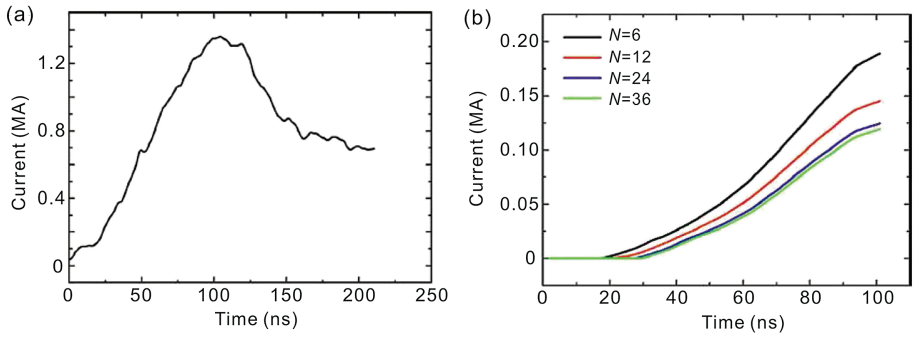

Fig. 7. (a) The total current on Qiangguang-1 facility. (b) The waveforms of current flowing through the plasmas inside the radius $r = 2.3$ mm for arrays with different wire numbers.

viscosity on the MRT instability in Z-pinches. Based on their work, we investigated the coupling effects of compressibility, viscosity and a sheared axial flow [59−63]. All these work helps us to understand the complexity and characteristics of Z-pinch instability.

To get a basic insight into the mode growth and an understanding of the physical mechanism driving the mode development, we used the 2D three-temperature MARED code [64] in (r, z) plane to study the implosion of an 8.75 mm radius, 1.0 mm thick shell with a single perturbation mode [65], and the drive condition is similar with those of the Saturn facility. The instability has been seeded by a density perturbation with wavelength $\lambda = 1.43$ mm and amplitude $A_0 = 0.5\%$. The temporal evolution of the FFT spectrum for the linear mass is shown in Fig. 8(a), and the simulated temporal growth of the fundamental amplitude, which is fitted with theoretical functions at different stages used in Haines' heuristic model [46], is shown in Fig. 8(b). In the linear stage (Zone I), the plasma boundary presents a typical sinusoidal outline, and the only mode could be found on the FFT spectrum is the initial one, whose growth rate remains exponential. During the "weak-nonlinear" stage (Zone II), the mode coupling happens between the basic and the 2nd harmonic, and the classical exponential function still fits well with the simulation results. The last stage is the deep-nonlinear one, which is characterized by the appearance of the 3rd and higher harmonics, resulted from the magnetic−plasma interaction. The magnetic field not only broadens its front into bubble structures, but also sharpens the lagged plasma tails into spikes.

For most previous 2D simulations, a random density seeding method has been used to simulate the initial perturbed plasma load. Numerical results illustrate that instabilities developed from different initial random seeds indeed have different imploding images, but their dominant modes before stagnation fluctuate slightly within a narrow range around 1.3 mm, which is consistent well with the experimental data gained from the fast-framing X-ray pinhole image in [66]. This indicates that the dominant mode is determined by the inner mechanism of the instability development, and has no direct relation to the microstructure of the certain load.

More investigations, such as the effect of the initial amplitude of the seeds to the final X-ray output, have also been conducted with parameters close to the Qiangguang-I facility. The drive current has a peak value of 1.4 MA at 162 ns, and the load parameters are height 2.0 cm and radius 4 mm. The initial amplitude of 0%, 10%, 20%, and 30% are used in the simulations. Fig. 9 shows the mesh of plasma at the stagnation and the dependence of the X-ray power to the initial amplitude. Clearly, as the initial seeds amplitude increases, the imploding shell is deformed severely, and the peak power output is reduced at the same time. However, the expansion of the full width at half maximum (FWHM) is not observed, which is a problem needs more attention in the future.

5. Stagnation and X-ray production

At the end of the implosion, the Z-pinch plasma collides on the axis and stagnates, which causes the implosion kinetic energy convert into plasma internal energy, and then large amounts of X-ray radiation are generated via a series of atomic transitions. The radiation can be produced by three mechanisms, i.e., spontaneous line emission, recombination radiation and bremsstrahlung radiation. Which process dominates Z-pinch x-ray radiation depends on many factors, such as the load parameters and the driving capability of the pulsed power accelerator.

Typically, two types of radiation sources are generated by wire-array Z-pinch implosions. One is to produce the sub-keV radiation by imploding high-Z wire-arrays, and this kind of radiation has an approximate Planckian spectrum and can be used for ICF studies. In the Z-pinch experiments performed by the China Academy of Engineering Physics on the low current facilities, X-ray radiation with peak powers from 0.5 TW to 5 TW and energies from 10 kJ to 100 kJ was generated [67,68], and the main processes can be replicated by simulations [69]. The other one is to produce the multi-keV K-shell X-ray radiation using low- to mid-Z wire-arrays, and this kind of radiation can be used for the research of radiation−material interaction.

The stagnation and radiation processes of Z-pinch implosion are studied mainly with two codes, the 2D three temperature MARED code [69] and the 1D nonequilibrium radiation CRMHA [70,71]. Fig. 10 shows the overall energy variation of an aluminum wire-array Z-pinch on a 7 MA level

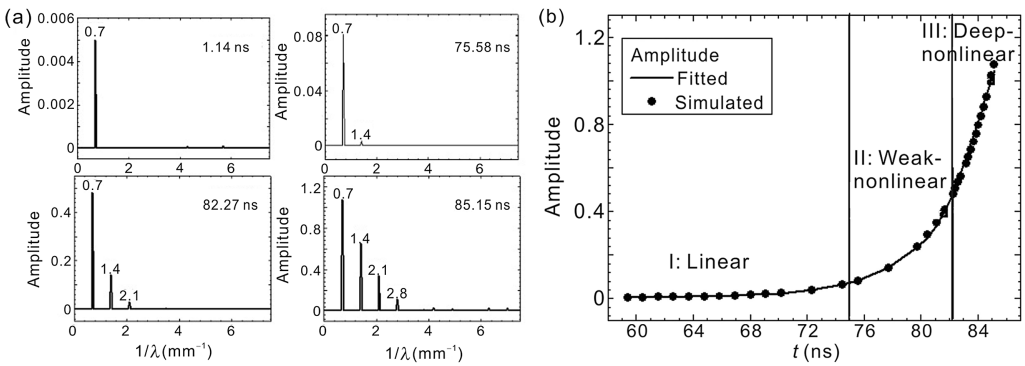

Fig. 8. (a)The temporal evolution of the FFT spectrum and mesh configuration for the single mode with $\lambda = 1.43$ mm and $A_0 = 0.5\%$; (b) Numerical amplitude evolutions for different stages and those fitted with theoretical or experiential functions.

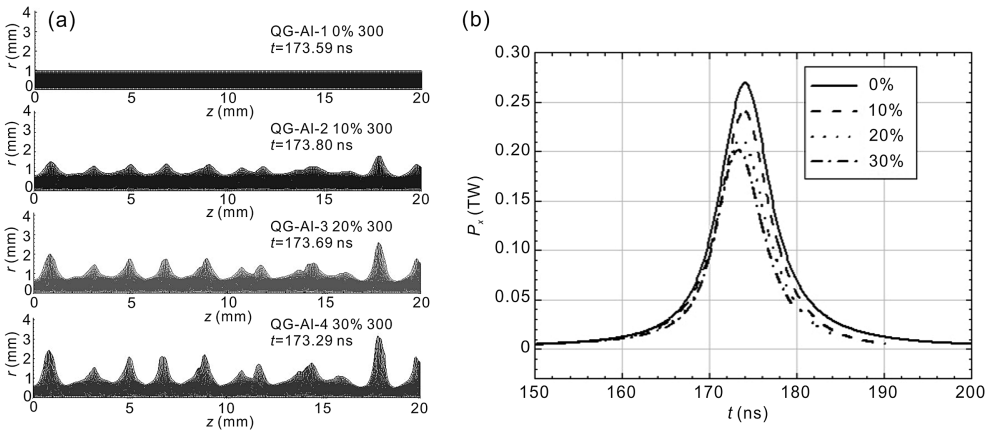

Fig. 9. (a) The mesh configuration before the stagnation and (b) the X-ray output for random seeds with different initial amplitude: 0%, 10%, 20%, 30%.

generator [72,73]. The generator feeds its stored energy to the load region via Poynting energy flux. Part of them is stored as magnetic energy, the other is converted into plasma kinetic energy by $\boldsymbol{J} \times \boldsymbol{B}$ work and thermal energy by Joule heat. When the plasma stagnates on the axis, plasma kinetic energy is converted to plasma thermal energy through pdV work and shock heating, thus producing the very high density and temperature plasma. At the same time powerful X-ray radiations are generated by strong electron-photon energy transition.

In different phases the plasma parameters change remarkably, so the dominating atomic processes and the corresponding radiation emission also vary largely. In the run-in phase of an aluminum Z-pinch implosion driven by 1.7 MA current the plasma is compressed and heated gradually [74]. With the increase of the electron temperature, the ionization and excitation processes principally determine the ion's populations, and then result in the population increase of excited states. Thus, the line emission increases and occupies a large part in total radiation. The characteristic line is optically thick and its self-absorption is very strong. On the contrary, photoionization and inverse bremsstrahlung absorption are relatively weak and the continuum is usually optically thin. So the share of line emission in total radiation decreases gradually in the run-in stage. However, in the stagnation phase the plasma is compressed to the state of very high density. As is known that the rate coefficient of three-body recombination is proportional to the square of the electron number density, and the free electron is mainly captured to the excited states. So the populations of some excited states, from which the most important lines can be emitted, reach the maximum in this phase. Consequently, the share of line emission increases again at stagnation. After the plasma expands gradually, the electron temperature and plasma density both decrease. And it is also known that the rate coefficient of radiative recombination is just proportional to the electron number density, and the free electron is mainly captured to the ground state in the transition. Hence, the decrease of radiative recombination is much weaker than that of three-body recombination, and then the population of excited states decreases rapidly, thus again leading to the decrease of the share of line emission in total radiation. Fig. 11 shows the populations of several ground states during the stagnation phase. It is shown that most ions are in the ground states of helium-like and lithium-like ionization stages during the production of the X-ray pulse. Hence, radiative recombination transited to the ground states of lithium-like and beryllium-like stages dominates the continuum. Additionally, the absolute yield of the line emission for a certain load is determined by the competition of the populations of excited states and the opacity effect, and the share of line emission is not fixed for different loads and accelerators.

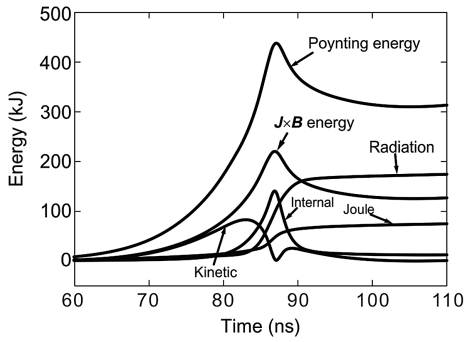

Fig. 10. Time history of energy terms in an aluminum Z-pinch implosion driven by a 7 MA current.

In order to explore the physics of K-shell radiation, we developed an ionization model with detailed configurations in hydrogen-like approximation, and five kinds of atomic transitions which determine the populations of energy levels are: 1) spontaneous emission and line absorption; 2) electron collisional excitation and de-excitation; 3) photoionization and radiative recombination; 4) collisional ionization and three-body recombination; 5) autoionization and dielectronic capture [70]. We then developed a non-equilibrium radiation MHD code coupled with this ionization model, and simulation results show that there are two necessary conditions for producing high yield of K-shell energy [71]. Firstly, highly ionized plasmas must be prepared before the beginning of

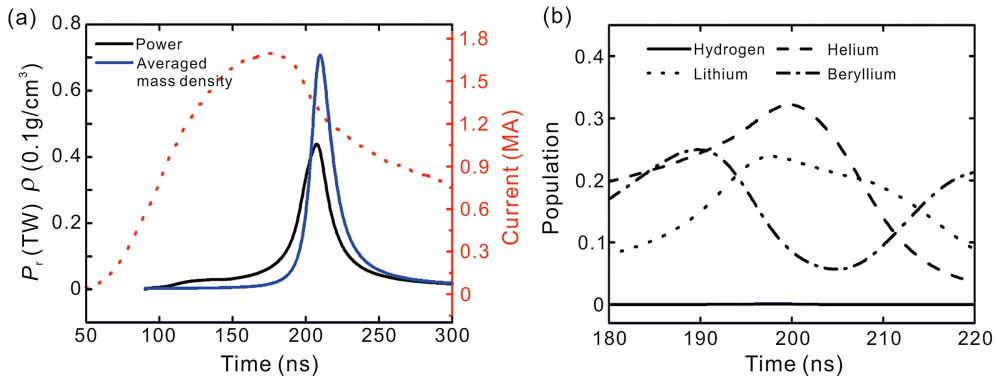

Fig. 11. (a) Variation of averaged mass density, calculated radiation power and the drive current with time. (b) Populations of ions in ground states of hydrogen-like(solid), helium-like(dashed), lithium-like(dotted), and beryllium-like(dash dotted) stages at stagnation.

recombination. Secondly, the density of the plasmas which are in recombination phase should be high enough.

Furthermore, our simulation results show that the maximum K-shell yield from a pure aluminum wire-array Z-pinch implosion can be obtained at an optimal load mass for a given generator and at a fixed initial wire-array radius. This optimal load mass is determined by the load energy coupling with the generator, the capability of Z-pinch plasmas to emit the K-shell radiation, and the self absorption of K-shell lines. When the optimal load mass increases for a higher current generator, the effect of line absorption shall be more important and limit the increase of K-shell yield. As is known, the line radiation is mainly absorbed in its line center, and the absorption in its wings is weaker. So we can use an alloyed wire-array with close atomic number elements to decrease the opacity effect and to increase the K-shell line emission [75,76]. In Fig. 12 the variations of the ratio of K-shell yield from an alloyed Al/Mg wire-array to that from a pure aluminum wire array with a_{Mg} for different generator are shown, where a_{Mg} is the mass share of magnesium. It is noted that in the case of 1.3 MA, even when the a_{Mg} is as high as 50 percent, the K-shell yield from an alloyed Al/Mg wire-array is just 12 percent higher than that from a pure aluminum wire-array. However, the K-shell yield increases over 19 percent as a_{Mg} increases to 10 percent with the drive current of 21 MA. Certainly, there exists a limit in the efficiency of improving the K-shell yield using alloyed Al/Mg wire-arrays. If the drive current is small and the optimal load mass is also relatively low, the increase of K-shell yield with alloyed Al/Mg wire-arrays will be less efficient.

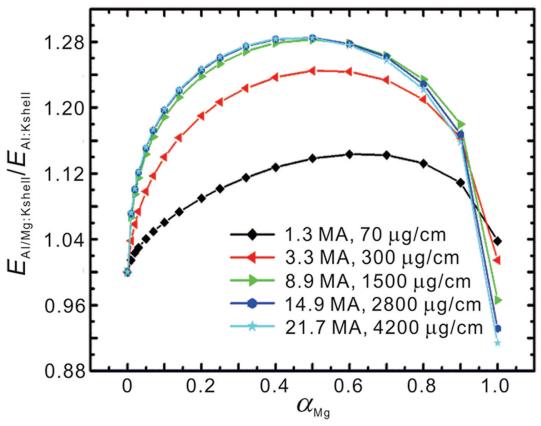

Fig. 12. Variation of the ratio of K-shell yield from an alloyed Al/Mg wire-array to that from a pure aluminum wire array with a_{Mg} for different generators.

6. Nested wire arrays

As mentioned above, the MRT instability during the wire array implosion is one of the primary impediments to achieve high X-ray power. A significant method to mitigate these instabilities is to introduce additional mass, such as an inner wire array, into the implosion plasmas [77].

A lot of experimental studies of nested wire array implosion have been carried out on facilities with different current level such as the Z, Saturn, MAGPIE, Angara-5-1 etc [78,79]. Three possible different implosion modes of nested wire array were suggested by Chittenden et al. [80]: (1) the hydrodynamic collision mode, (2) the transparent inner mode, and (3) flux compression mode. Based on Grabovskii's theory, a modified thin shell model combined with equivalent circuit equations was developed by Ding et al. [18], and was used to obtain different implosion modes by changing the length of inner array, in Fig. 13. Esaulov et al. analyzed the hydrodynamic collision mode and the transparent inner mode with a wire dynamics model (WDM) [79], which was then updated into the WADM model [81] with effects due to the ablated plasma.

However, these methods are all based on the thin shell assumption, and the effects from wire number and interwire gaps are neglected. To get a more comprehensive understanding of the nested array dynamics, 2D MHD models in (r, θ) geometry are more suitable. By using a two dimensional magnetohydrodynamic (2D MHD) model in (r, θ) geometry, Chittenden et al. studied the implosion process of the transparent inner mode [80]. Douglas et al. established a

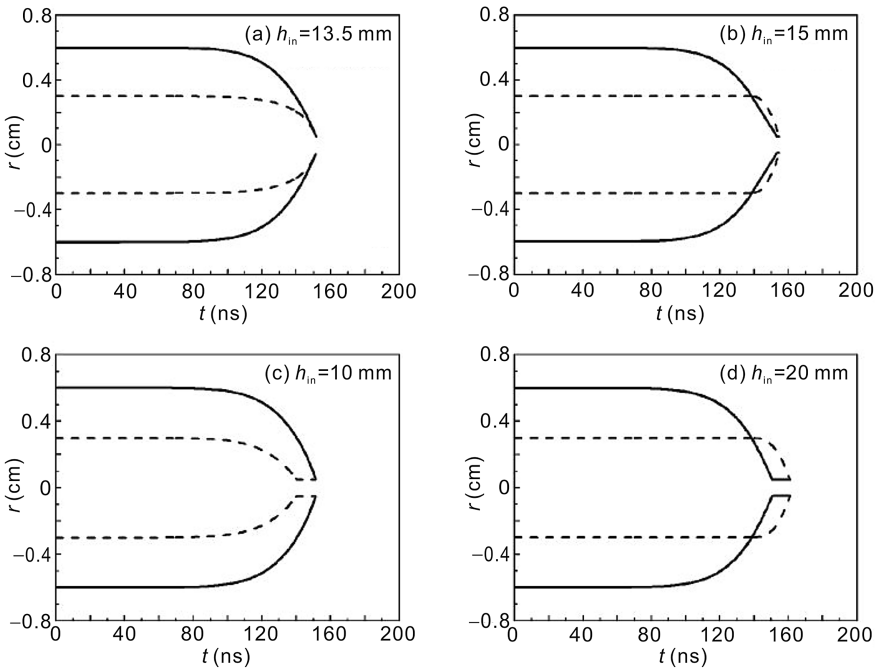

Fig. 13. Four implosion modes of nested wire-arrays with different initial inner wire length. (a) Outer array impacts the inner one, and both reach the axis together; (b) Inner and outer array reach the axis at the same time; (c) Inner array reaches the axis firstly; (d) Transparent inner mode.

2D (r, z) MHD model to simulate the hydrodynamic collision mode, and the development of MRT instability during implosion was described. However, these MHD simulations can be used to study the implosion process for a certain mode.

We studied the influence of the wire number of outer array on the implosion mode of nested wire array by using a 2D (r, θ) resistive MHD code [82] which has been used to simulate the implosion process of single wire array [19]. The current distribution inside the wire array depends not only on the inductance, but also on the diffusion and convection of magnetic field in the array plasmas. The wire number of outer array can affect the dynamics and thermodynamics of plasmas inside the array, and thereby influence the current distribution and the implosion process of nested wire array. Thus, the MHD simulation results will be different from that of the thin shell calculations even if the driven conditions and initial load parameters are the same.

Simulation results show that the implosion modes of nested wire array can be changed obviously by only adjusting the wire number of the outer array when the other conditions are fixed. With a 5 MA current, three different implosion modes predicted by other researchers are obtained by choosing the wire number of the inner array to be 16 and the outer array to be 16, 64, and 88 respectively, while the thin shell simulation results show that the implosion modes for these three cases should be the same (see Fig. 14). Fig. 15 shows the implosion process for the nested array with 64 outer wires. In this case, the small interwire gap of the outer array leads to an obvious screen effect, which prevents significant current flow in the inner array at early times. The outer array carries about 80% of the total discharge current at $t = 20$ ns, and starts to implode at about $t = 60$ ns, while the inner array is still static. At about 90 ns, the inner array begins to move towards the axis when the outer one has reached the radial position about $r = 0.4$ cm. About 10 ns later, the outer array plasmas collide with the inner array and then both arrays move toward the axis together, and finally reach the minimum radius about $r = 0.05$ cm at $t = 105$ ns. Before and after the collision, the implosion velocity of the outer array is about 3.45×10^7 cm/s and 2.44×10^7 cm/s respectively. The implosion behavior of the nested array is close to the hydrodynamic collision mode.

Furthermore, we found that the larger the interwire gap of the outer array is, the more important the effects of discrete wires will be, and the difference between results from the MHD and the thin shell models will be greater. So it is more reasonable to predict the implosion mode of nested wire array by using 2D (r, θ) model especially for those whose wire number is relative small and effect of discrete wire is hard to be neglected.

It should be noticed that in our MHD simulations, the initial diameter and temperature of plasma corona are given artificially, which could influence the ablation and implosion process of wire plasmas thereby affect the implosion modes. Therefore, to predict the implosion mode accurately, the description of explosion process of single wire at the early stage of discharge should be included. By combining the implosion mode with the analysis of MRT instability, design of optimum load parameters for the implosion of nested wires array is possible. Furthermore, our 2D resistive MHD model in (r, θ) geometry can be applied to the other wire array configurations where the current distribution is also important, such as planar arrays etc. We will carry out these researches in our future works.

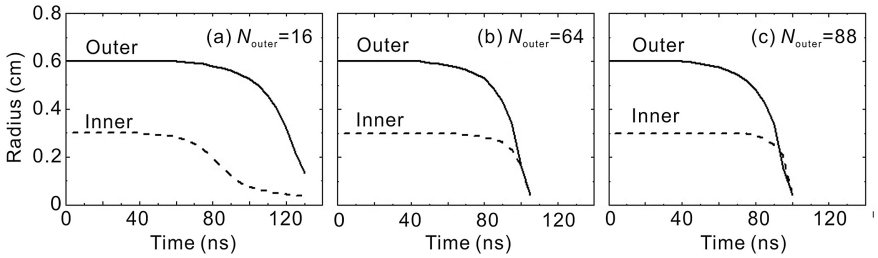

Fig. 14. Implosion trajectory of outer and inner array for the wire arrays with (a) $N_{in} = 16$ and $N_{outer} = 16$; (b) $N_{in} = 16$ and $N_{outer} = 64$; (c) $N_{in} = 16$ and $N_{outer} = 88$.

7. Quasi-spherical implosion

The key point of Z-pinch dynamic hohlraum (ZPDH) [83–86] is to get a high efficient transition of energy from an imploding Z-pinch plasma to a cylindrical low-density foam convertor, and then create a high-temperature hohlraum radiation for the ICF capsule ignition [4–8]. However, the radiation energy absorbed by the capsule is insufficient yet for the fusion ignition, and the search for a more effective use of the kinetic energy of imploding liner pinch is still attractive.

One of the potential methods is to change the cylindrical implosion into a spherical one, in which the plasma concentrates on the center, instead of the axis of symmetry [87]. Simulation results from Nash et al. [88–90] and Smirnov et al. [87] showed that, in a spherical DH system the hohlraum radiation temperature increases considerably. A double shell quasi-spherical (QS) system designed for the 28 MA ZR machine was simulated by Nash et al., which produced volumetric ignition of the inner deuterium-tritium (DT) target and a yield of 12 MJ [89,90].

Since the magnetic field on the surface of a spherical load is naturally nonuniform, one has to counterbalance its effect by reasonable design. The conventional method is to modulate the areal mass density with the latitude θ as $m(\theta) \propto 1/\cos^2\theta$. This so-called mass-redistribution method was proved feasible by a series of experiments on the 9 μs, 12 MA Shiva Star accelerator [91,92], but does not work with wire-arrays and short pulse generators used for ZPDH study. Previous attempts on the Angara5-I [87] and MAGPIE generators did not show compelling evidence of QS implosions with wire-arrays.

As a solution to the abovementioned problem, we developed a new method of realizing QS implosions with wire-arrays, in which the mass-redistribution is replaced by shape-modification [93]. Fig. 16(a) shows a possible scheme of a reshaped load, of which the initial surface satisfies the parabola function as

$$xr_0 + \alpha z^2 = r_0^2,$$

where $\alpha = 0.3$ is the parameter determining the initial shape of the load. By increasing the imploding distance for the load with the magnitude of the latitude, we expect every part of the load will implode to the center simultaneously. Fig. 16(b) shows the simulated density evolvement of the reshaped load.

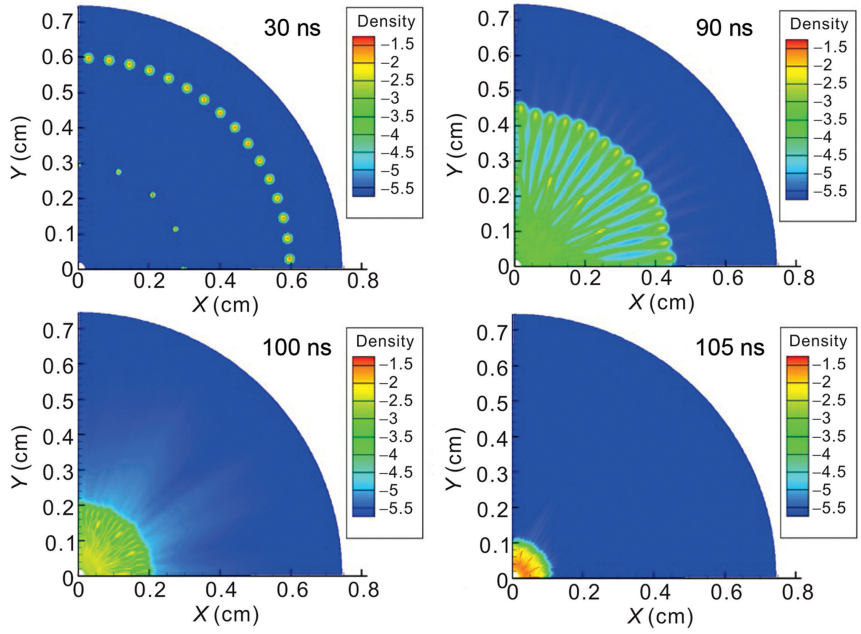

Fig. 15. Contours of logarithm of mass density at different time for the case with $N_{in} = 16$ and $N_{outer} = 64$.

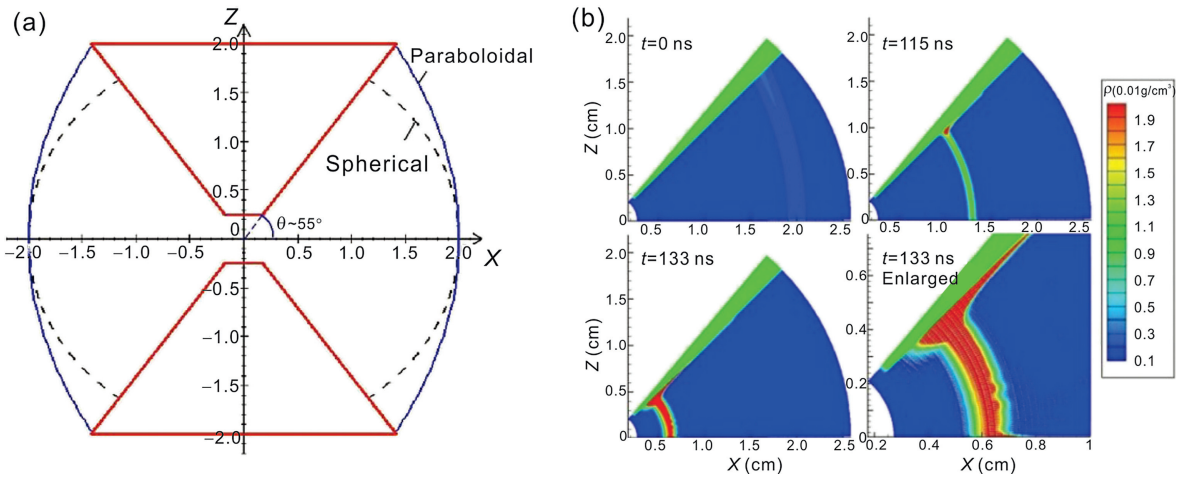

Fig. 16. (a) Configuration of a prolate quasi-spherical load. (b) Density evolution for a 2.0 cm, $\pm 45^{o}$ QS load with $\alpha = 0.3$.

The drive current has a peak of 28 MA, and the rise time is 69 ns. During the implosion, the load changes its shape gradually from a prolate sphere to a regular one. Plasmas near the electrode catch up those near the equator ultimately due to faster acceleration and higher speed. At $t = 133$ ns, the load becomes spherical and the inner boundary reaches about $r = 0.6$ cm, and the distribution of velocity vector shows great uniformity. Simulation results also suggest that the implosion quality of the prolate sphere load is susceptive to their initial shape. To ensure the symmetry and quality of the QS implosion, it would be necessary to develop techniques that can control the load initial shape effectively and precisely.

Experiments on the 1.5 MA Qiangguang-I facility investigated the relationship between the loads initial shape and the final implosion quality. Self-emitting X-ray and ultraviolet images obtained in the experiments confirmed that the implosion quality is sensitive to the initial shape of the load, defined by the ratio of load height to diameter (H/d), and it is feasible to get QS implosions with wire arrays, which are pre-shaped properly (see Fig. 17, also in [94]).

We also investigated the impact of quasi-spherical implosion on a foam convertor. To ensure that all the imploding plasma reach the foam convertor almost at the same time, loads with different initial shapes are investigated numerically. Simulation results show that for a 4 mm diameter foam target, the optional H/d range of wire arrays in Fig. 17 is 1.18~1.28, which corresponds to a impact time disagreement of $\delta t \leq 3$ ns. Another issue to be discussed for the QSDH design is the shape of the foam target. Since the inherent non-uniform kinetic energy E_k of quasi-spherical implosions increases with the latitude [93], which results in uneven shock propagation in the foam target, ellipsoidal foam targets are more suitable to encounter the higher shock speed in the axial direction than those spherical ones. Fig. 18 shows a set of self-emitting X-ray pinhole images of implosion with $H/d = 1.18$, and the foam diameter is 3.85 mm. The simulated density profiles with ±30% density perturbation seeds are shown as well. The main body of the imploding plasma has an obvious deformation from its initial shape. Spike-like structures near the outer surface suggest a spherically inward movement. The radiation on the foam target surface is not uniform, and two bright points of emission are observed at the foam-electrode gaps due to the locally high current density and self-pinching process. After $t = +6.9$ ns, an axially dominated compression of the foam can be observed, which qualitatively agrees with the numerical results. Agreed with our expectation, experimental results with prolate ellipsoidal foam targets show more uniform compression, and the calculated implosion velocity and its impact on the foam target agree well with the measurement. More experimental results and detailed analysis can be found in [95].

8. Dynamic hohlraum and dynamic hohlraum driven ICF

High efficiency of energy conversion of Z-pinch implosions also makes the fast Z-pinch a possible selection for driving ICF. One approach is the magnetized liner inertial fusion [10], in which a beryllium liner is imploded to directly compress the DT fuel, and the fuel is magnetized by an external current coil and preheated by a laser pulse to lower the required convergence. Another approach is to indirectly compress a fusion capsule by hohlraum radiation irradiation. Several hohlraum configurations have been suggested and extensively explored [83]. The double Z-pinch hohlraum uses two Z-pinch implosions to produce two identical primary hohlraums, and the radiation fluxes both from the primary hohlraums and Z-pinch plasmas are transferred into the secondary hohlraum, in which a fusion capsule is placed. A more efficient hohlraum is the dynamic hohlraum [96], which is typically produced after a tungsten wire-array impacts onto a low density CH converter embedded on the axis of the wire-array. If a fusion capsule is inserted at the center of the axis, it will be compressed by the hohlraum radiation.

Simulations show that a local high pressure region, which is generated by the impaction of the tungsten plasma with the converter plasma, is crucial to launch the strongly radiating shock wave and to form the dynamic hohlraum. Due to the supersonic radiation transfer in the low opacity CH converter

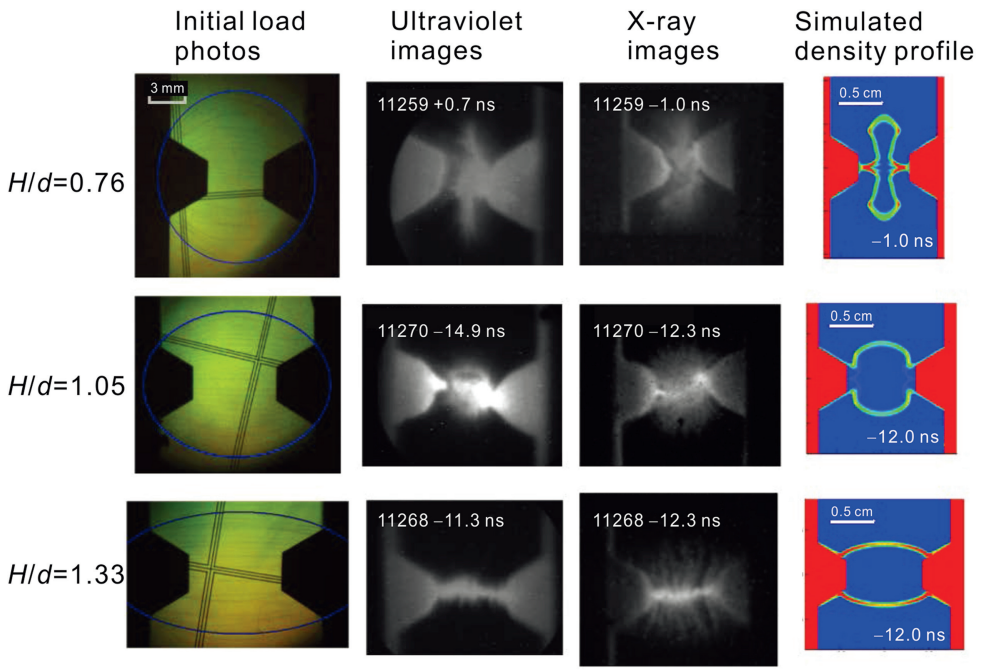

Fig. 17. Initial load images, self-emitting ultraviolet images, X-ray images, and simulated density profiles at late implosion for loads with $H/d = 0.76$, 1.05, and 1.33, respectively. The blue curves in the initial load photos are used to sketch out the outlines of the wire array.

plasma, which is also produced in the high pressure region, there exists a hohlraum region inside the front of the shock wave, in which the radiation is high. Basically, the hohlraum radiation is determined by the detailed profiles of plasma conditions when the wire-array plasma impacts onto the CH converter plasma. And these profiles are determined by many factors, such as the drive current, initial masses and radii of the wire-array and the converter, as well as the material of the converter. Fig. 19 shows the variations of shock fronts and hohlraum radiation temperature as the mass ratio of the wire-array to the CH converter is varied with peak current of 8 MA [97]. It is shown that as this ratio is increased, the shock velocity is increased and the radiation temperature is increased as well. Additionally, the time duration of the radiation pulse before the shock arrives at the axis is remarkably increased. It is found that when this mass ratio is slightly lower than unity, for example 0.75, a relative optimal dynamic hohlraum can be produced. It is also found that a suitable radius ratio of the wire-array to the converter, neither too large, inducing strong MRT instability, nor too small, gaining a small kinetic energy of the wire-array before impacting onto the converter surface, should be selected. Our recent results also show the possibility of optimizing the dynamic hohlraums by covering the low density converter with a thin and relatively high density converter.

For a low current generator, it is difficult to generate high temperature hohlraums. But the collision interaction can be carefully examined by imploding a light wire-array onto a

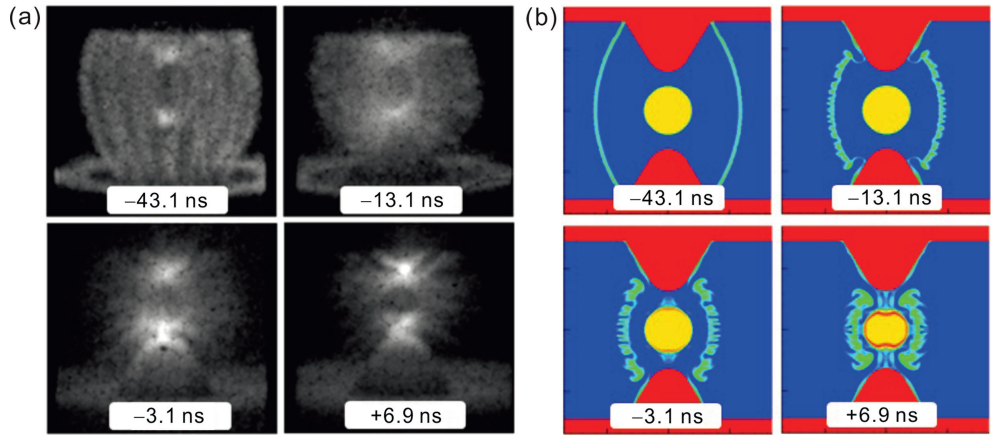

Fig. 18. Self-emitting X-ray pinhole images (a) and the simulated density profiles (b) at $t = -43.1$ ns, -13.1 ns, -3.1 ns, $+6.9$ ns, $+11.9$ ns, and $+16.9$ ns (according to the time of peak current).

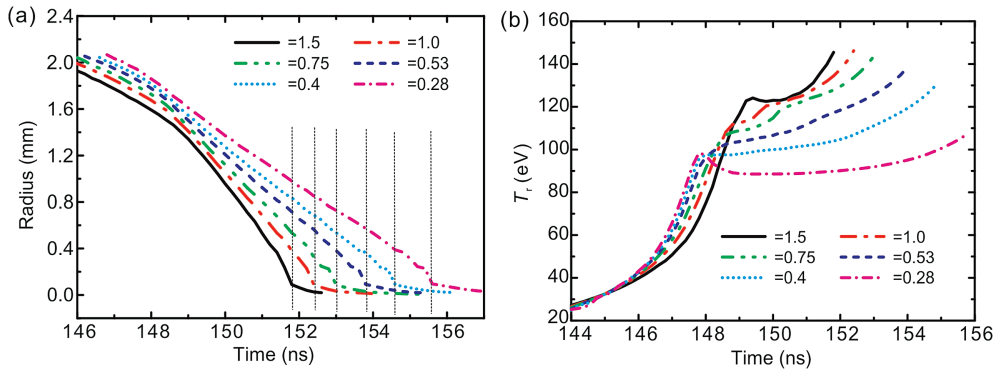

Fig. 19. Variations of shock trajectories (a) and hohlraum radiation temperatures (b) with the time as the mass ratio of the wire-array to the converter is varied.

relatively heavy converter, in which the time interval between the collision and stagnation will be largely increased. In recent years, the experiments using a relative light wire-array embedded with a heavy foam converter were performed on the 1.5 MA Qiangguang-I facility [98]. The collision and stagnation processes were observed and a two-peak radial radiation pulse was produced. Experimental results also showed a higher ratio of the first peak to the second peak in the case of larger wire-array radius. Fig. 20 compares the foam boundary from simulations with that from two types of experiments, in which the initial radius of the wire-array is varied. It is shown that the measured processes of compression, stagnation and expansion of the foam converter correspond well with the simulation results.

We have performed one- and two-dimensional simulations of dynamic hohlraum driven capsule implosion. Typically, the Z-pinch implosion and the dynamic hohlraum are cylindrical. The fusion capsule is composed of a low Z ablator and the DT fuel, and the capsule implosion is needed to be spherical to gain high compression. Once the hohlraum radiation transfers to the ablator surface, it is heated up to form an ablation shock to propagate inward. The shocked ablator shell will drive the compression of the fuel. Meanwhile, the hohlraum shock generated in the converter plasma will continue to propagate to the ablator plasma and may finally compress the fuel. The fuel compression due to radiation ablation is relatively symmetrical at the equator and poles. However, the fuel is only compressed at the equator by the cylindrical shock, which means that the shock compression is completely asymmetric.

To gain symmetrical fuel compression driven by hohlraum radiation ablation and avoid asymmetric shock compression is a crucial issue for driving ICF using dynamic hohlraums. As we know, the shock pressure qualitatively varies linearly with the material temperature, and the ablation pressure varies as 3.5 power of the hohlraum radiation temperature. Therefore, as the hohlraum temperature increases, the ablation pressure will eventually exceed the shock pressure, and then the expansion of the ablated plasma will obviously weaken the shock propagation and decrease its velocity after the shock transferring into the ablator plasma. Consequently, longer time duration is provided for the symmetrical target implosion driven by radiation ablation. Our numerical results, whether by changing drive currents or by varying load parameters, clearly validate this mechanism [99]. In our simulations, a critical hohlraum radiation temperature of over 140 eV is needed to provide a high enough ablation pressure to decelerate the hohlraum shock. When the drive current is smaller than 10 MA, such as 5 MA or 8 MA, the hohlraum radiation temperature (with a target) is less than 120 eV. In these cases, the ablated plasma only has a weak effect on decelerating the hohlraum shock, and the target implosion driven by radiation ablation is hardly isolated from shock compression. When the

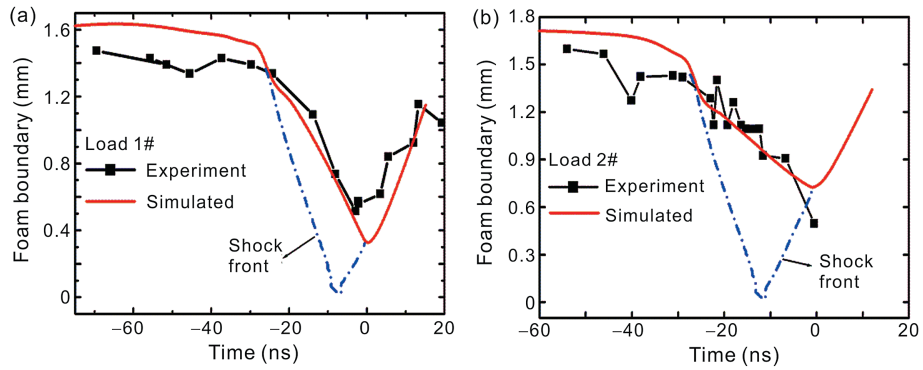

Fig. 20. Comparison of the simulated foam boundary with that measured by multi-shot shadowgraphs for wire-array Z-pinch implosions(load 1# and 2#) embedded with the same foam converter on the Qiangguang-I facility.

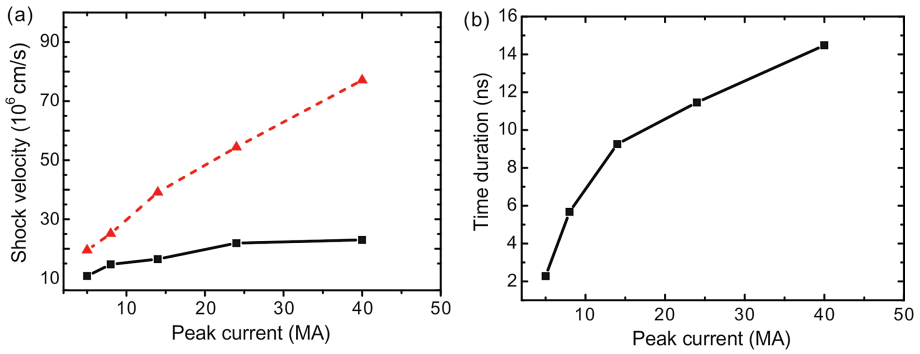

Fig. 21. (a) Variation of hohlraum shock velocities with the drive current before(triangle) and after(square) the hohlraum shock propagates over the converter/ablator plasma. (b) Variation of hohlraum time duration with the drive current before the shock reaches the fuel surface.

drive current is over 14 MA, the ablation pressure can be increased to be comparable to or greater than the shock pressure, thus possibly isolating the target implosion from the shock. As the drive current is increased, the hohlraum shock can be decelerated much more, and the longer time duration for pure radiation ablation is obtained, as shown in Fig. 21. In the cases of 14 MA and 40 MA, the velocity of the hohlraum shock after propagating into the ablator plasma is largely decreased, only 42.2 percent and 29.8 percent of that before propagating in the converter plasma. As a result, the time duration, during which the fuel can be compressed by radiation ablation with the hohlraum shock away from the fuel surface, is increased from 7.1 ns to 10.3 ns. If the drive current is further increased, longer time duration can be provided for symmetrical radiation ablation in ICF ignition researches.

We also performed two-dimensional integrated simulations of dynamic hohlraum driven capsule implosion, and the overall processes from the wire-array implosion, hohlraum formation, radiation ablation to the final neutron production are gained. Fig. 22 shows a typical two-dimensional simulation result of dynamic hohlraum driven target implosion. The cylindrical hohlraum is formed by the collision of the wire-array plasma with the foam converter, and the corresponding hohlraum radiation drives the spherical target (a CH ablator + DD fuel) to implode inward. It is shown that the movement of the ablator is affected not only by the symmetrical radiation ablation, but also by the asymmetrical cylindrical shock. However, due to the time delay of the shock to the fuel surface after it is decelerated in the ablator plasma, the fuel is just compressed by the hohlraum radiation irradiation.

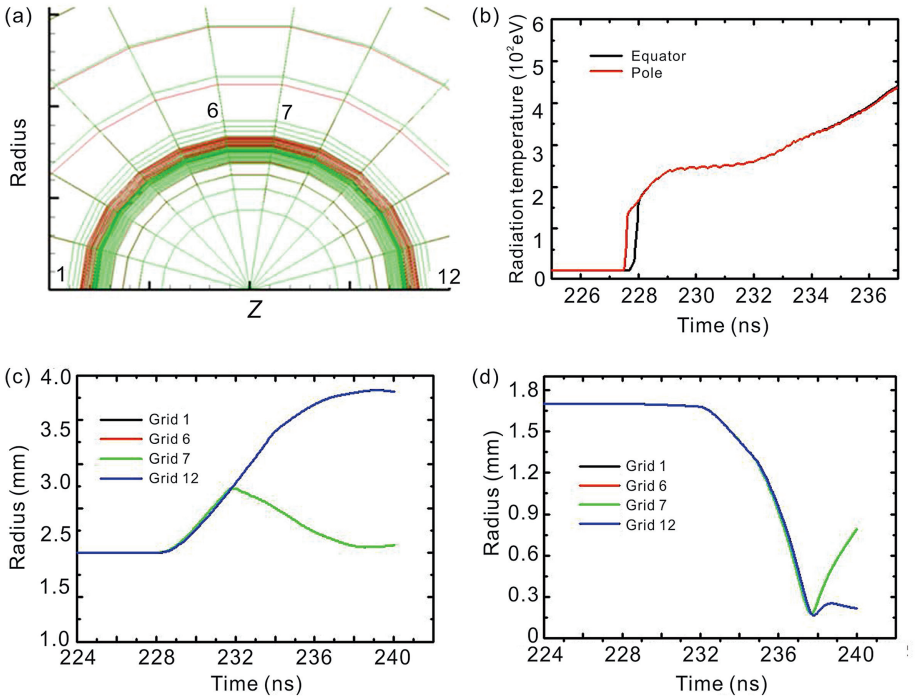

Fig. 22. (a) Grid schematic of two-dimensional dynamic hohlraum driven target implosion. (b) variation of hohlraum radiation temperature at the equator and pole of the ablator surface. (c) Trajectories of ablator surfaces in equator(6,7) and in pole(1,12). (d) Trajectories of fuel surfaces in equator(6,7) and in pole(1,12).

Therefore the compression of the fuel is nearly symmetrical in the equator and in poles.

In future we will further concentrate on the optimization of dynamic hohlraums and the design of dynamic hohlraum driven inertial fusion.

9. Conclusion

In this paper we presented an overview of the theoretical and computational investigations of wire array Z-pinches performed at the Institute of Applied Physics and Computational Mathematics. Key processes of the wire-array Z-pinch implosion, including the wire ablation and precursor formation, the implosion and MRT instability, the stagnation and radiation, are investigated with different models and numerical codes. The implosion of nested wire arrays and quasi-spherical wire arrays are studied as an alternative choice for driving the ICF ignition. Based on these works, we have achieved a comprehensive understanding of the wire-array Z-pinch physics, and recently more attention is paid on the ZPDH study. Fundamental processes, such as the wire-foam impact, creation of hohlraum radiation, and the ICF capsule implosion, were investigated numerically with various 1D and 2D RMHD codes, which showed us a primary image of the ZPDH drive ICF. However, these codes and their numerical results need to be confirmed and verified by further experimental data, which is the main work in the near future. Additionally, the new proposed MagLIF concept arises our interest, and reminds us to pay more attention on the new methods and concepts of using Z-pinch in the inertial fusion energy.

Acknowledgments

This work is supported by the National Natural Science Fund of China (Nos. 11405012, 10975022, 11275030, 11105017, 11135007, 11471047, 91330107), the Foundation of President of China Academy of Engineering Physics (No.2014-1-042) and the Defense Industrial Technology Development Program (B1520133015).

References

[1] N.R. Pereira, J. Davis, N. Rostoker, X-rays from Z-pinches on relativistic electron-beam generators, J. Appl. Phys. 64 (1988) R1−R27.
[2] R.B. Spielman, C. Deeney, G.A. Chandler, M.R. Douglas, D.L. Fehl, et al., Tungsten wire-array Z-pinch experiments at 200 TW and 2 MJ, Phys. Plasmas 5 (1998) 2105−2111.
[3] C. Deeney, M.R. Douglas, R.B. Spielman, T.J. Nash, D.L. Peterson, et al., Enhancement of X-ray power from a Z pinch using nested-wire arrays, Phys. Rev. Lett. 81 (1998) 4883−4886.
[4] T.J. Nash, M.S. Derzon, G.A. Chandler, R. Leeper, D. Fehl, et al., High-temperature dynamic hohlraums on the pulsed power driver Z, Phys. Plasmas 6 (1999) 2023−2029.
[5] S.A. Slutz, M.R. Douglas, J.S. Lash, R.A. Vesey, G.A. Chandler, et al., Scaling and optimization of the radiation temperature in dynamic hohlraums, Phys. Plasmas 8 (2001) 1673−1691.
[6] J. Bailey, G. Chandler, S. Slutz, G.R. Bennett, G. Cooper, et al., X-ray imaging measurements of capsule implosions driven by a Z-pinch dynamic hohlraum, Phys. Rev. Lett 89 (2002), 095004.
[7] S.A. Slutz, J.E. Bailey, G.A. Chandler, G.R. Bennett, G. Cooper, et al., Dynamic hohlraum driven inertial fusion capsules, Phys. Plasmas 10 (2003) 1875−1882.
[8] C.L. Ruiz, G.W. Cooper, S.A. Slutz, J.E. Bailey, G.A. Chandler, et al., Production of thermonuclear neutrons from deuterium-filled capsule implosions driven by Z-pinch dynamic hohlraums, Phys. Rev. Lett. 93 (2004) 015001.
[9] G.A. Rochau, J.E. Bailey, G.A. Chandler, G. Cooper, G.S. Dunham, et al., High performance capsule implosions driven by the Z-pinch dynamic hohlraum, Plasma Phys. Control. Fusion 49 (2007) B591.
[10] S.A. Slutz, M.C. Herrmann, R.A. Vesey, A.B. Sefkow, D.B. Sinars, et al., Pulsed-power-driven cylindrical liner implosions of laser preheated fuel magnetized with an axial field, Phys. Plasmas 17 (2010) 056303.
[11] C. Xue, N. Ding, S. Sun, D. Xiao, Y. Zhang, et al., Full circuit model for coupling pulsed power driver with Z-pinch load, Acta Phys. Sin. 63 (2014) 125207.
[12] L. Wang, J. Wu, N. Guo, J. Han, M. Li, et al., Investigation of the resistance and inductance of planar wire array at Qiangguang accelerator, Plasma Sci. Technol. 14 (2012) 842−846.
[13] L.B. Yang, H.D. Liao, C.W. Sun, K. Ouyang, J. Li, et al., RT instability in cylindrical implosion of jelly ring, Chin. Phys. 13 (2004) 1747.
[14] S. Zhao, C. Xue, X. Zhu, R. Zhang, H. Luo, et al., Determining the resistance of X-pinch plasma, Chin. Phys. B 22 (2013) 045205.
[15] J. Deng, W. Xie, S. Feng, M. Wang, H. Li, et al., Initial performance of the primary test stand, IEEE Trans. Plasma Sci. 41 (2013) 2580−2583.
[16] W. Zou, F. Guo, L. Chen, S. Song, M. Wang, et al., Full circuit calculation for electromagnetic pulse transmission in a high current facility, Phys. Rev. ST Accel. Beams 17 (2014) 110401.
[17] C. Xue, N. Ding, Y. Zhang, D. Xiao, S. Sun, et al., Full circuit simulation for electromagnetic pulse forming and transforming in the PTS facility, High Power Laser Part. Beams 28 (2016) 014014.
[18] N. Ding, Y. Zhang, Q. Liu, D. Xiao, X. Shu, et al., Effects of various inductances on the dynamic models of the Z-pinch implosion of nested wire arrays, Acta Phys. Sin. 58 (2009) 1083−1090.
[19] J. Huang, N. Ding, C. Xue, S. Sun, Two-dimensional magnetohydrodynamic studies of implosion modes of nested wire array Z-pinches, Phys. Plasmas 21 (2014) 072707.
[20] L. Yin, J. Wu, Y. Yao, A cell functional minimization scheme for parabolic problem, J. Comput. Phys. 229 (2010) 8935−8951.
[21] L. Yin, J. Wu, Y. Yao, A cell functional minimization scheme for domain decomposition method on non-orthogonal and non-matching meshes, Numer. Math. 128 (2014) 773−804.
[22] J. Wu, Z. Gao, Z. Dai, A stabilized linearity-preserving scheme for the heterogeneous and anisotropic diffusion problems on polygonal meshes, J. Comput. Phys. 231 (2012) 7152−7169.
[23] Z. Gao, J. Wu, A small stencil and extremum-preserving scheme for anisotropic diffusion problems on arbitrary 2D and 3D meshes, J. Comput. Phys. 250 (2013) 308−331.
[24] J. Wu, Z. Gao, Interpolation-based second-order monotone finite volume schemes for anisotropic diffusion equations on general grids, J. Comput. Phys. 275 (2014) 569−588.
[25] L. Yin, J. Wu, Z. Gao, The cell functional minimization scheme for the anisotropic diffusion problems on arbitrary polygonal grids, ESAIM M2AN 49 (1) (2015) 193−220.
[26] Z. Gao, J. Wu, A second-order positivity-preserving finite volume scheme for diffusion equations on general meshes, SIAM J. Sci. Comput. 37 (1) (2015) A420−A438.
[27] T.W.L. Sanford, G.O. Allshouse, B.M. Marder, T.J. Nash, R.C. Mock, et al., Improved symmetry greatly increases X-ray power from wire-array Z-pinches, Phys. Rev. Lett. 77 (1996) 5063−5066.
[28] T.W.L. Sanford, R.C. Mock, R.B. Spielman, D.L. Peterson, D. Mosher, et al., Increased X-ray power generated from low-mass large-number aluminum-wire-array Z-pinch implosions, Phys. Plasmas 10 (1998) 3737−3754.
[29] V.V. Aleksandrov, E.V. Grabovski, A.N. Gribov, G.M. Oleinik, A.A. Samokhin, et al., Transportation of an electromagnetic pulse to the load in the angara-5-1 facility, Plasma Phys. Rep. 34 (2008) 911−919.

[30] S.V. Lebedev, F.N. Beg, S.N. Bland, J.P. Chittenden, A.E. Dangor, et al., Snowplow-like behavior in the implosion phase of wire array Z-pinches, Phys. Plamsas 9 (2002) 2293−2301.
[31] C.A. Jennings, J.P. Chittenden, M.E. Cuneo, W.A. Stygar, D.J. Ampleford, et al., Circuit model for driving three-dimensional resistive MHD wire array Z-pinch calculations, IEEE Trans. Plasma Sci. 36 (2010) 529−539.
[32] M.E. Cuneo, E.M. Waisman, S.V. Lebedev, J.P. Chittenden, W.A. Stygar, et al., Characteristics and scaling of tungsten-wire-array Z-pinch implosion dynamics at 20 MA, Plasma Phys. Rep. 71 (2005) 046406.
[33] E.V. Grabovski, G.G. Zukakishvili, K.N. Mitrofanov, G.M. Oleinik, I.N. Frolov, et al., Study of the magnetic fields and soft X-ray emission generated in the implosion of double wire arrays, Plasma Phys. Rep. 32 (2010) 32−46.
[34] S.V. Lebedev, F.N. Beg, S.N. Bland, J.P. Chittenden, A.E. Dangor, et al., Effect of discrete wires on the implosion dynamics of wire array Z-pinches, Phys. Plasmas 8 (2001) 3734−3747.
[35] J.B. Greenly, J.D. Douglass, D.A. Hammer, B.R. Kusse, S.C. Glidden, et al., A 1 MA, variable risetime pulse generator for high energy density plasma research, Rev. Sci. Instrum. 79 (2008) 073501.
[36] V.V. Alexsandrov, A.V. Branitskii, G.S. Volkov, E.V. Grabovskii, M.V. Zurin, et al., Dynamics of heterogeneous liners with prolonged plasma creation, Plasma Phys. Rep. 27 (2001) 89−109.
[37] P.V. Sasorov, B.V. Oliver, E.P. Yu, T.A. Mehlhorn, One-dimensional ablation in multiwire arrays, Phys. Plasmas 15 (2008) 022702.
[38] E.P. Yu, B.V. Oliver, D.B. Sinars, T.A.M.M.E. Cuneo, et al., Steady-state radiation ablation in the wire-array Z-pinch, Phys. Plasmas 14 (2007) 022705.
[39] E.P. Yu, M.E. Cuneo, M.P. Desjarlais, R.W. Lemke, D.B. Sinars, et al., Three-dimensional effects in trailing mass in the wire-array Z pinch, Phys. Plasmas 15 (2008) 056301.
[40] S.C. Bott, S.V. Lebedev, D.J. Ampleford, S.N. Bland, J.P. Chittenden, et al., Dynamics of cylindrically converging precursor plasma flow in wire-array Z-pinch experiments, Phys. Rev. E 74 (2006) 046403.
[41] F.N. Beg, S.V. Lebedev, S.N. Bland, J.P. Chittenden, A.E. Dangor, et al., The dynamics of single and nested nickel wire array Z-pinch implosions, IEEE Trans. Plasma Sci. 30 (2002) 552−558.
[42] J. Huang, S. Sun, N. Ding, C. Ning, D. Xiao, et al., Numerical studies of ablated-plasma dynamics and precursor current of wire-array Z-pinches, Phys. Plasmas 18 (2011) 042704.
[43] J. Huang, S. Sun, D. Xiao, N. Ding, C. Ning, et al., Two-dimensional numerical studies of ablated-plasma dynamics of wire-array Z-pinches, Acta Phys. Sin. 59 (2010) 6351−6361.
[44] S. Lebedev, D. Ampleford, S. Bland, S. Bott, J. Chittenden, et al., Implosion dynamics of wire array Z-pinches: experiments at Imperial College, Nucl. Fusion 44 (12) (2004). S215.
[45] C. Ning, S.K. Sun, D.L. Xiao, Y. Zhang, N. Ding, et al., Numerical studies of the effects of precursor plasma on the performance of wire-array Z-pinches, Phys. Plamsas 17 (2010) 062703.
[46] M.G. Haines, A heuristic model of the wire array Z-pinch, IEEE Trans. Plasma Sci. 26 (1998) 1275−1281.
[47] D.L. Peterson, R.L. Bowers, J.H. Brownell, A.E. Greene, K.D. McLenithan, et al., Two-dimensional modeling of magnetically driven Rayleigh Taylor instabilities in cylindrical Z-pinches, Phys. Plasmas 3 (1996) 368−381.
[48] D.L. Peterson, R.L. Bowers, K.D. McLenithan, C. Deeney, G.A. Chandler, et al., Characterization of energy flow and instability development in two-dimensional simulations of hollow Z-pinches, Phys. Plasmas 5 (1996) 3302−3310.
[49] T.W. Hussey, N.F. Roderick, U. Shumlak, R.B. Spielman, C. Deeney, et al., A heuristic model for the nonlinear Rayleigh-Taylor instability in fast Z-pinches, Phys. Plasmas 2 (1995) 2055−2062.
[50] R. Latham, J.A. Nation, F.L. Curzon, A. Folkierski, Growth of surface instabilities in a linear pinched discharge, Nature 186 (1960) 624−625.
[51] R.L. Bowers, G. Nakafuji, A.E. Greene, K.D. McLenithan, D.L. Peterson, et al., Two-dimensional modeling of X-ray output from switched foil implosions on Procyon, Phys. Plasmas 3 (1996) 3448−3468.
[52] T.W.L. Sanford, R.C. Mock, B.M. Marder, T.J. Nash, R.B. Spielman, et al., Variation of high-power aluminum-wire array Z-pinch dynamics with wire number, load mass, and array radius, AIP Conf. Proc. 409 (1997) 561−573.
[53] D.L. Peterson, R.L. Bowers, J.H. Brownell, C. Lund, W. Matuska, et al., Application of 2-D simulations to hollow Z-pinch implosions, AIP Conf. Proc. 409 (1997) 201−210.
[54] J.H. Hammer, J.L. Eddleman, P.T. Springer, M. Tabak, A. Toor, et al., Two-dimensional radiation-magnetohydrodynamic simulations of SATURN imploding Z-pinches, Phys. Plasmas 3 (1996) 2063−2069.
[55] M.R. Douglas, C. Deeney, N.F. Roderick, Effect of sheath curvature on Rayleigh-Taylor mitigation in high-velocity uniform-fill, Z-pinch implosions, Phys. Rev. Lett. 78 (1997) 4577−4580.
[56] X.M. Qiu, L. Huang, G.D. Jian, Finite Larmor radius magnetohydrodynamic analysis of the Rayleigh-Taylor instability in Z-pinches with sheared axial flow, Phys. Plasmas 14 (2007) 032111.
[57] X.M. Qiu, L. Huang, G.D. Jian, Mitigation effect of finite Larmor radius on Rayleigh-Taylor instability in Z-pinch implosions, Chin. Phys. Lett. 19 (2002) 217−219.
[58] X.M. Qiu, L. Huang, G.D. Jian, Stabilization of viscosity on Rayleigh-Taylor instability in Z-pinches, Chin. Phys. Lett. 21 (2004) 689−692.
[59] Y. Zhang, N. Ding, The mitigation effect of sheared axial flow on the Rayleigh-Taylor instability in Z-pinch plasma, Nucl. Fusion & Plasma Phys. 25 (2005) 15−21.
[60] Y. Zhang, N. Ding, Effects of compressibility on the magneto-Rayleigh-Taylor instability in Z-pinch implosions with sheared axial flows, Phys. Plasmas 13 (2006) 022701.
[61] Y. Zhang, N. Ding, The effect of axial flow on the stability in the Z-pinch, Acta Phys. Sin. 55 (2006) 2333−2339.
[62] Y. Zhang, N. Ding, Stability analysis of viscous Z-pinch plasma with a sheared axial flow, Chin. Phys. B 17 (2008) 2994−3002.
[63] N. Ding, Y. Zhang, Q. Liu, Simplified analysis of the MHD instability in Z-pinch plamas, Nucl. Fusion Plasma Phys. 28 (2008) 101−104.
[64] N. Ding, J. Wu, Z. Yang, S. Fu, C. Ning, et al., Simulation of Z-pinch implosion using MARED code, High Power Laser Part. Beams 20 (2008) 212−218.
[65] Y. Zhang, J. Wu, Z. Dai, N. Ding, C. Ning, et al., Computational investigation of the magneto-Rayleigh-Taylor instability in Z-pinch implosions, Phys. Plasmas 17 (2010) 042702.
[66] T.W.L. Sanford, T.J. Nash, R.C. Mock, R.B. Spielman, K.W. Struve, et al., Dynamics of a high-power aluminum-wire array Z-pinch implosion, Phys. Plasmas 4 (2010) 2188−2203.
[67] N. Ding, C. Ning, Z. Wang, Z. Li, R. Xu, et al., X-ray radiation power optimization in 1 MA to 4 MA wire-array implosions, Acta Phys. Sin. 60 (2011) 025209.
[68] N. Ding, R. Xu, Z. Li, J. Yang, S. Jiang, et al., New results of sino-russian joint Z-pinch experiments, Acta Phys. Sin. 60 (2011) 045208.
[69] N. Ding, J. Wu, Z.H. Yang, S.W. Fu, C. Ning, et al., Simulation of Z-pinch implosion using MARED code, High Power Laser Part. Beams 20 (2008) 212.
[70] K. Lan, Y. Zhang, W. Zheng, Theoretical study on discharge-pumped soft X-ray laser in Ne-like Ar, Phys. Plasmas 6 (4343) (1999).
[71] K. Lan, Y. Zhang, Theoretical studies of aluminum wire array Z-pinch implosions with varying masses and radii, Eur. Phys. J. AP 19 (2002) 103.
[72] D. Xiao, C. Ning, K. Lan, N. Ding, Preliminary studies of the mechanism of producing radiation in aluminum wire array Z-pinch implosion, Acta Phys. Sin. 59 (2010) 430.
[73] D. Xiao, N. Ding, C. Ning, K. Lan, Non-equilibrium radiation of aluminum wire array Z-pinch, High Power Laser Part. Beams 22 (2010) 341.
[74] D. Xiao, N. Ding, C. Ning, S. Sun, Y. Zhang, et al., Numerical investigation on the X-ray production of aluminum-wire-array z-pinch implosion, IEEE Trans. Plasma Sci. 39 (2011) 686.
[75] C. Deeney, P.D. Lepell, B.H. Failor, S.L. Wong, J.P. Apruzese, et al., Increased kilo-electron-volt X-ray yields from Z-pinch plasmas by mixing elements of similar atomic numbers, Phys. Rev. E 51 (1995) 4823−4832.

[76] D. Xiao, N. Ding, C. Xue, J. Huang, Y. Zhang, et al., Increasing the k-shell yield of line radiation in Z-pinch implosions using alloyed al/mg wire-arrays, Phys. Plasmas 20 (2013) 013304.
[77] N.A.G.J. Davis, A.L. Velikovich, Fast commutation of high current in double wire array Z-pinch loads, Appl. Phys. Lett. 70 (1997) 170−172.
[78] S.V. Lebedev, R. Aliaga-Rossel, S.N. Bland, J.P. Chittenden, A.E. Dangor, et al., Two different modes of nested wire array Z-pinch implosions, Phys. Rev. Lett. 84 (2000) 1708−1711.
[79] A.A. Esaulov, A.L. Velikovich, V.L. Kantsyrev, T.A. Mehlhorn, M.E. Cuneo, Wire dynamics model of the implosion of nested and planar wire arrays, Phys. Plasmas 13 (2006) 120701.
[80] J.P. Chittenden, S.V. Lebedev, S.N. Bland, A. Ciardi, M.G. Haines, The different dynamical modes of nested wire array Z-pinches, Phys. Plasmas 8 (2001) 675−678.
[81] A.A. Esaulov, V.L. Kantsyrev, A.S. Safronova, A. L.Velikovich, I.K. Shrestha, et al., Wire ablation dynamics model and its application to imploding wire arrays of different geometries, Phys. Rev. E 86 (2012) 046404.
[82] J. Huang, N. Ding, C. Ning, S. Sun, Y. Zhang, et al., Numerical investigation on the implosion dynamics of wire-array Z-pinches in (r, θ) geometry, Phys. Plasmas 19 (2012) 062701.
[83] M. Matzen, Z pinches as intense X-ray sources for high-energy density physics applications, Phys. Plasmas 4 (1997) 1519−1527.
[84] R. Leeper, T. Alberts, J. Asay, P.M. Baca, K.L. Baker, et al., Z-pinch driven inertial confinement fusion target physics research at Sandia National Laboratories, Nucl. Fusion 39 (1999) 1283−1294.
[85] J. Hammer, M. Tabak, S.C. Wilks, J.D. Lindl, D.S. Bailey, et al., High yield inertial confinement fusion target design for a Z-pinch-driven hohlraum, Phys. Plasmas 6 (1999) 2129−2136.
[86] M. Cuneo, D. Sinars, E. Waisman, D.E. Bliss, W.A. Stygar, et al., Compact single and nested tungsten-wire-array dynamics at 14c19 MA and applications to inertial confinement fusion, Phys. Plasmas 13 (2006) 056318.
[87] V. Smirnov, S. Zakharov, E. Grabovskii, Increase in radiation intensity in a quasi-spherical double liner/dynamic hohlraum system, JETP Lett. 81 (2005) 442−447.
[88] T. Nash, D. McDaniel, R. Leeper, C.D. Deeney, T.W.L. Sanford, et al., Design, simulation, and application of quasi-spherical 100 ns Z-pinch implosions driven by tens of mega-amperes, Phys. Plasmas 12 (2005) 052705.
[89] T. Nash, P. VanDevender, D. McDaniel, L. Abbot, Quasi-spherical Direct Drive Fusion, Sandia National Laboratory Report No.SAND 2007−0235.
[90] P. VanDevender, D. McDaniel, N. Roderick, T. Nash, Quasi-spherical Direct Drive Fusion Simulations for the Z Machine and Future Accelerators, Sandia National Laboratory Report No. SAND2007−7178.
[91] J. Degnan, F. Lehr, J. Beason, G.P. Baca, D.E. Bell, et al., Electromagnetic implosion of spherical liner, Phys. Rev. Lett. 74 (1995) 98−101.
[92] J. Degnan, M. Alme, B. Austin, J.D. Beason, S.K. Coffey, et al., Compression of plasma to megabar range using imploding liner, Phys. Rev. Lett. 82 (1999) 2681−2684.
[93] Y. Zhang, N. Ding, Z. Li, S. Sun, C. Xue, et al., Dynamics of quasi-spherical Z-pinch implosions with mass redistribution and displacement modification, Phys. Plasmas 19 (2012) 122704.
[94] Y. Zhang, N. Ding, Z. Li, R. Xu, S. Sun, et al., Numerical study of quasi-spherical wire-array implosions on the Qiangguang-i facility, IEEE Trans. Plasma Sci. 40 (2012) 3360−3366.
[95] Y. Zhang, N. Ding, Z. Li, R. Xu, D. Chen, et al., Realization of quasi-spherical implosion using pre-shaped prolate wire arrays with a compression foam target inside, Phys. Plasmas 22 (2015) 020703.
[96] J.H. Brownell, R.L. Bowers, K.D. McLenithan, D.L. Peterson, Radiation environments produced by plasma z -pinch stagnation on central targets, Phys. Plasmas 5 (1998) 2071.
[97] D. Xiao, S. Sun, C. Xue, Y. Zhang, N. Ding, et al., Numerical studies on the formation process of Z-pinch dynamic hohlruams and key issues of optimizing dynamic hohlraum radiation, Acta Phys. Sin. 64 (2015) 235203.
[98] D. Xiao, N. Ding, F. Ye, J. Ning, Q. Hu, et al., Numerical and experimental investigations on the interaction of light wire-array z-pinches with embedded heavy foam converters, Phys. Plasmas 21 (2014) 042704.
[99] D. Xiao, S. Sun, Y. Zhao, N. Ding, J. Wu, et al., Numerical investigation on target implosions driven by radiation ablation and shock compression in dynamic hohlraums, Phys. Plasmas 22 (2015) 052709.